Article

Not peer-reviewed version

Quantitative Assessment of the Trigger Effect of Proton Flux on Seismicity

Alexey Lyubushin * and Eugeny Rodionov

Posted Date: 27 March 2025

doi: 10.20944/preprints202503.2031.v1

Keywords: earthquakes; proton flux; point processes; wavelets; kurtosis; spectral slope; entropy; multifractals

 doi:10.20944/preprints202503.2031.v1

Article

Quantitative Assessment of the Trigger Effect of Proton Flux on Seismicity

Alexey Lyubushin * and Eugeny Rodionov

Institute of Physics of the Earth RAS, Moscow 123242, Russia; evgeny_980@list.ru
* Correspondence: lyubushin@yandex.ru

Abstract: An estimate of the trigger effect of the proton flux on seismicity is obtained. The proton flux time series with a time step of 5 minutes, 2000-2024, is analyzed. In each time interval of 5 days, statistics of the proton flux time series are calculated: mean values, logarithm of kurtosis, spectral slope, singularities spectrum support width, wavelet-based entropy and the Donoho-Johnston wavelet based index. For each of the used statistics, time points of local extrema were found and for each pair of time sequences of proton flux statistics and earthquakes with a magnitude of at least 6.5 in sliding time windows, the "advance measures" of each time sequence relative to the other were estimated using a model of the intensity of interacting point processes. The difference between the "direct" measure of the advance of time points of local extrema of proton flux statistics relative to the time moments of earthquakes and the "inverse" measure of the advance was calculated. The maximum proportion of the intensity of seismic events for which the proton flux is a trigger is estimated as 0.28 for using the points of the local minima of the singularities spectrum support width.

Keywords: earthquakes; proton flux; point processes; wavelets; kurtosis; spectral slope; entropy; multifractals

1. Introduction

The influence of solar activity on various processes on Earth has long been the subject of close study, which resulted in the appearance of the term "space weather". The review [1] considers various aspects of the influence of solar activity on the Earth's climate and anthropogenic processes. The ionosphere, as an important component of the concept of space weather, was studied in the works [2–4]. The results of the development of statistical methods for predicting strong solar flares, including using machine learning, are presented in the articles [5–8]. An important issue in the study of space weather is its impact on catastrophic events in the life of society, such as earthquakes. In particular, methods have not yet been developed that allow us to unambiguously answer the question of whether strong solar flares and other electromagnetic events in the ionosphere have a trigger effect on the occurrence of sufficiently strong earthquakes. A lot of research is devoted to this issue [9]. The papers [10,11] present the results of the analysis of correlations between 11-12-year cycles of solar activity and time intervals of increasing intensity of seismic events over long periods of time. A comparison of time intervals of high seismic activity with the phases of solar cycles since 1900 is carried out in the paper [12].

The identification of the effects of the delay of strong earthquakes relative to the time intervals of geomagnetic storm maxima was considered in [13,14]. In [15], a similar effect of the delay of seismic events was studied for sunspot numbers. The hypothesis about the occurrence of time anomalies of atmospheric electric fields preceding the occurrence of strong earthquakes, including deep-focus ones, as a result of processes in the source of an impending seismic event was studied in [16]. A similar question about the occurrence of atmospheric and ionospheric electromagnetic signals recorded by spacecraft and preceding moderate seismic events was considered in [17]. In [18,19], the

 doi:10.20944/preprints202503.2031.v1

difference between the global seismic process and the Poisson one after excluding aftershocks is explained by the piezoelectric effect in rocks as a result of the impact of the proton flux during solar activity, which has a periodic time structure in addition to the 11-12-year solar cycle. In [20–22], the hypothesis is investigated about the generation of telluric currents in the earth's crust as a result of the impact of disturbances of ionospheric electromagnetic fields from solar flares and, as a consequence, their trigger effect on the foci of future seismic events. A statistical analysis of the impact of 50 largest solar flares in the time interval 1997–2024 on global seismic activity was performed in [23], as a result of which an increase in seismic activity was discovered within 10 days after the flare compared to 10 days before it. The paper [24] provides an overview of the work in Russia for the period 1995-2020 on the study of the influence of artificial and natural electromagnetic impacts on seismicity and discusses possible ways of using electromagnetic seismicity to reduce seismic hazard. The classification of seismic events with a magnitude of at least 6 as they occur as a result of the impact of a proton flux using a neural network was performed in the paper [25].

The complex dynamics of both the Sun and solar-terrestrial relations requires the use of a set of modern data processing methods based on the use of nonlinear models for the analysis of time series describing interacting systems [26]. In [27,28], the internal dynamics of solar cycles was studied using methods of empirical orthogonal oscillation modes, estimates of their maximum Lyapunov exponents and entropy flows between the values of various parameters of processes inside the Sun. In [29,30], various estimates of the Hurst exponent and entropy measures were used to analyze data obtained using the Swarm satellite network of the European Space Agency to describe the most intense magnetic storms and to quantitatively study the complexity of processes in the upper ionosphere. In [31], a study was conducted of the structure of currents induced by geomagnetic storms, leading to accidents in electrical networks, by applying information theory and various entropy measures to their time series.

In this paper, a new method is proposed that allows obtaining a quantitative estimate of the influence of various statistics of the proton flux density time series measured by the Solar Heliospheric Observatory (SOHO) [32] on the sequence of earthquakes with a magnitude of at least 6.5. The method is based on the use of estimates of "advance measures" based on a parametric model of the intensities of interacting point processes and on the calculation of wavelet measures of spectral tilt and entropy, as well as on an estimate of the width of the carrier of the multifractal spectrum of singularities of the proton flux density time series.

2. Proton Flux Initial Data

The time series of proton flux values with a time step of 5 minutes was downloaded from the website [33]. Figure 1 shows a graph of the time series of proton flux density for the time period from the beginning of 2000 to October 17, 2024. The time step is 5 minutes.

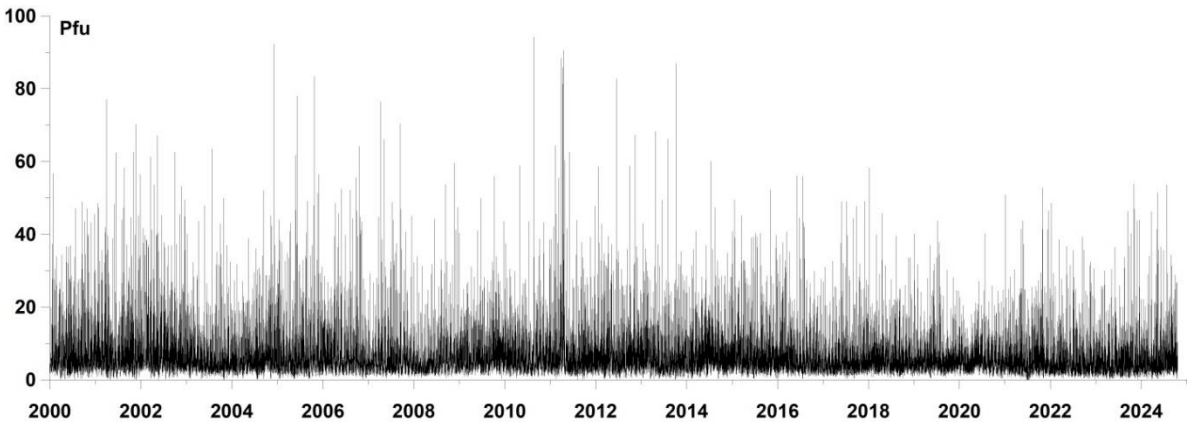

Figure 1. Time series graph of the proton flux from the beginning of 2000 to October 17, 2024 with a time step of 5 minutes. Proton flux density unit “Pfu” means Particles·cm^{-1}·sec^{-1}·steradian^{-1}.

 doi:10.20944/preprints202503.2031.v1

In the future, when analyzing the relationship between the proton flux and earthquakes, we will use various statistics of the proton flux density time series calculated in a time interval of 5 days (1440 readings with a time step of 5 minutes), taken with an offset of 1 day (288 5-minute readings).

We start with the simplest statistics equal to the average value of the flux density in these intervals. From the beginning of 2000 to October 17, 2024, 1136 earthquakes with a magnitude of at least 6.5 occurred. Therefore, we find the 1136 largest local maxima of the average flux density values and present them as a function of the position of the right end of 5-day time windows. These two time sequences of events are shown in Figure 2.

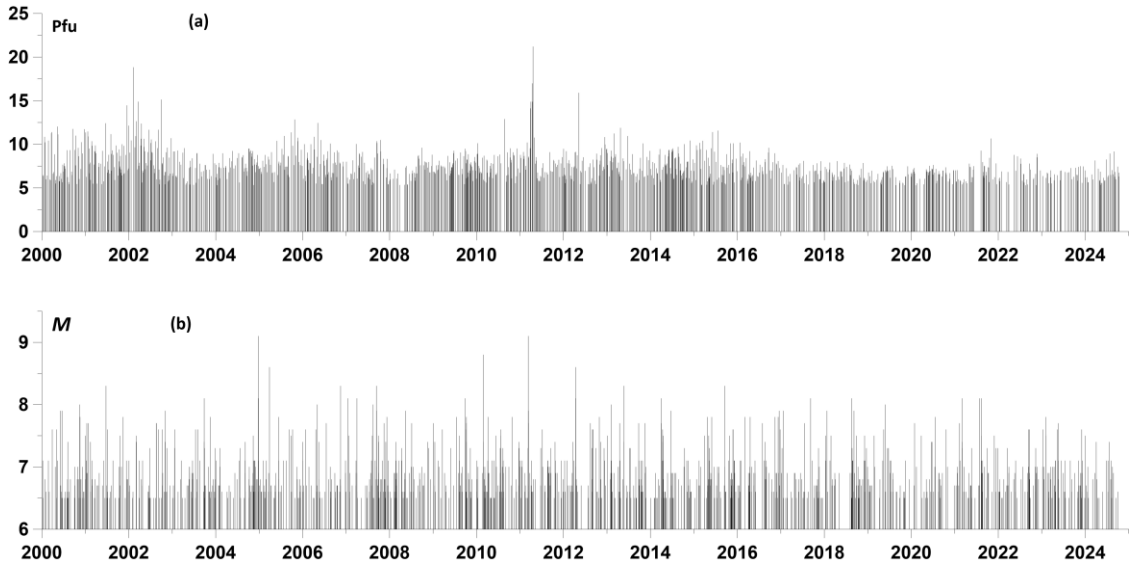

Figure 2. (a) – time sequence of 1136 largest local maxima of average values of proton flux density in sliding time windows of 5 days with a shift of 1 day; (b) – time sequence of earthquakes with a magnitude of at least 6.5, data from the source [34].

3. Periodic Components of the Proton Flux

The proton flux comes from the Sun, for which a number of periodicities are known, the best known of which is the 11-12-year periodicity, which determines the numbering of solar cycles. However, there is also a period due to the rotation of the Sun around its axis, equal to approximately 27 days. This periodicity should be reflected in variations in the proton flux density. Figure 3 shows the spectral composition of the proton flux density after the transition from the original time series to the average daily values. The power spectrum of the proton flux was calculated in a sliding time window of 730 days (2 years) with an offset of 30 days using the autoregressive model of order 70 [35]. The time-frequency diagram of the evolution of the spectrum logarithm is shown in Figure 3(a), while the values obtained by averaging the spectral estimates from all time windows are presented as a graph in Figure 3(b). This figure highlights 4 maximum spectral peaks, next to which the values of their periods in days are indicated. It is evident that the maximum spectral peak has a period of 26.95 days, approximately equal to the period of the Sun's rotation. The other periods correspond to its overtones.

 doi:10.20944/preprints202503.2031.v1

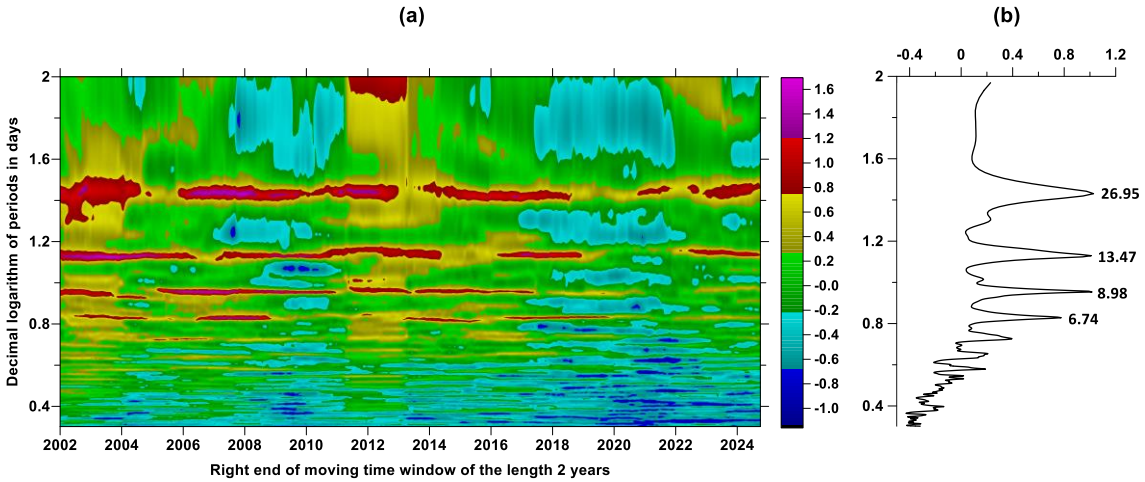

Figure 3. Spectral composition of the proton flux in the low-frequency part of the spectrum: (a) – frequency-time diagram of the evolution of the logarithm of the power spectrum in a sliding time window of 2 years; (b) – graph of the average power spectrum from all time windows, the period in days is shown next to the 4 largest spectral peaks.

4. Periodic Components of the Earthquake Sequence

Of interest is the question of whether the 27-day periodicity of the proton flux shown in Figure 2 is reflected in the periodicity of the intensity of seismic events. To do this, it is necessary to estimate this periodicity, taking into account that the sequence of earthquakes is not a time series with a constant time step, for which classical spectral estimation methods [35] can be applied. Below, the method proposed in [36] is used to estimate the periodic components of the intensity of the sequence of events. In [37], this method was used to calculate the periodic component of the stepwise variations in the time series of the displacement of the earth's surface measured by GPS.

Let $t_i, i=1,...,N$ be the times of the sequence of events observed on the interval $(0,T]$. Consider the following intensity model containing a periodic component:

$$\lambda(t) = \mu \cdot (1 + a\cos(\omega t + \varphi)) \tag{1}$$

where frequency ω, amplitude $a, 0 \le a \le 1$, phase angle φ, and $\varphi \in [0, 2\pi]$ multiplier $\mu > 0$ (describing the Poisson part of the intensity) are parameters of the model. Thus, the Poisson part of the intensity is modulated by a harmonic oscillation. Let us fix some value of frequency ω. The logarithmic likelihood function [38] in this case for a series of observed events is equal to:

$$\begin{aligned} \ln(L) &= \sum_{t_i} \ln(\lambda(t_i)) - \int_0^T \lambda(s)ds = \\ &= N\ln(\mu) + \sum_{t_i} \ln(1 + a\cos(\omega t_i + \varphi)) - \mu T - \frac{\mu a}{\omega}[\sin(\omega T + \varphi) - \sin(\varphi)] \end{aligned} \tag{2}$$

Taking the maximum of expression (2) with respect to the parameter μ, it is easy to find that:

$$\ln(L(\hat{\mu}, a, \varphi \mid \omega)) = \sum_{t_i} \ln(1 + a\cos(\omega t_i + \varphi)) + N \cdot \ln(\hat{\mu}(a, \varphi \mid \omega)) - N \tag{4}$$

It should be noted that the expression $\hat{\mu}(a = 0, \varphi \mid \omega) \equiv \hat{\mu}_0 = N/T$ is an estimate of the intensity of the process under the condition that it is Poisson homogeneous (purely random). Thus, the increment of the logarithmic likelihood function due to the consideration of a richer intensity model with a harmonic component with a given frequency ω than for a purely random flow of events is equal to:

$$\Delta \ln L(a, \varphi \mid \omega) = \sum_{t_i} \ln(1 + a\cos(\omega t_i + \varphi)) + N \cdot \ln(\hat{\mu}(a, \varphi \mid \omega)/\hat{\mu}_0) \tag{5}$$

Let

 doi:10.20944/preprints202503.2031.v1

$$R(\omega) = \max_{a,\varphi} \Delta \ln L(a, \varphi \,|\, \omega), \;\; 0 \le a \le 1, \varphi \in [0, 2\pi] \tag{6}$$

An important issue when applying this method to real data is determining the statistical significance of the obtained peak values of statistics (6). Let us consider two hypotheses for the same data set $X^{(N)}$ consisting of independent observations:

1) $X^{(N)}$ distributed by density $p_0(X^{(N)} \,|\, \theta_0)$ - hypothesis H_0;

2) $X^{(N)}$ distributed by density $p_1(X^{(N)} \,|\, \theta_1)$ - hypothesis H_1.

where θ_0 and θ_1 are vectors of unknown parameters, having dimensions m_0 and m_1, and the hypothesis H_1 is more "rich": $m_1 > m_0$, and the vector of parameters θ_1 completely includes the components of the vector θ_0. Let us consider the difference between the logarithms of the likelihood for these two hypotheses, provided that the vectors of parameters are taken from their maximum likelihood estimates:

$$\Delta \ln L(X^{(N)}) = \ln\left(\max_{\theta_1} p_1(X^{(N)} \,|\, \theta_1)\right) - \ln\left(\max_{\theta_0} p_0(X^{(N)} \,|\, \theta_0)\right) \tag{7}$$

It is evident that $\Delta \ln L(X^{(N)}) \ge 0$. According to Wilks' theorem [39], if the hypothesis is true, the quantity (7) has an asymptotic distribution:

$$\Delta \ln L(X^{(N)}) \sim \frac{\chi^2_m}{2}, \quad m = m_1 - m_0, \quad N \to \infty \tag{8}$$

In our case $m = 2$ and therefore, the doubled value (8) has an asymptotic distribution density χ^2_2 equal to $e^{-x/2}/2$, and the value (8) itself is distributed asymptotically as

$$\text{Prob}\{R(\omega) < x\} = 1 - e^{-x}, \quad N \to \infty \tag{9}$$

provided that the analyzed sequence of time moments is distributed according to the Poisson law with constant intensity. Expression (9) allows us to set thresholds for statistics that allow us to assert that only when they are exceeded does the sequence of time moments differ from the Poisson sequence with a given probability.

For a time sequence of seismic events with a magnitude of at least 6.5 (Figure 2(b)) we calculate the increments of the logarithmic likelihood function (6) in a sliding time window of 730 days (2 years) with a shift of 30 days for 200 frequency values ω corresponding to the values of periods varying from 10 to 100 days with a uniform step in a logarithmic scale. The resulting frequency-time dependence, similar to the usual spectral frequency-time diagram in Figure 3(a), is shown in Figure 4(a).

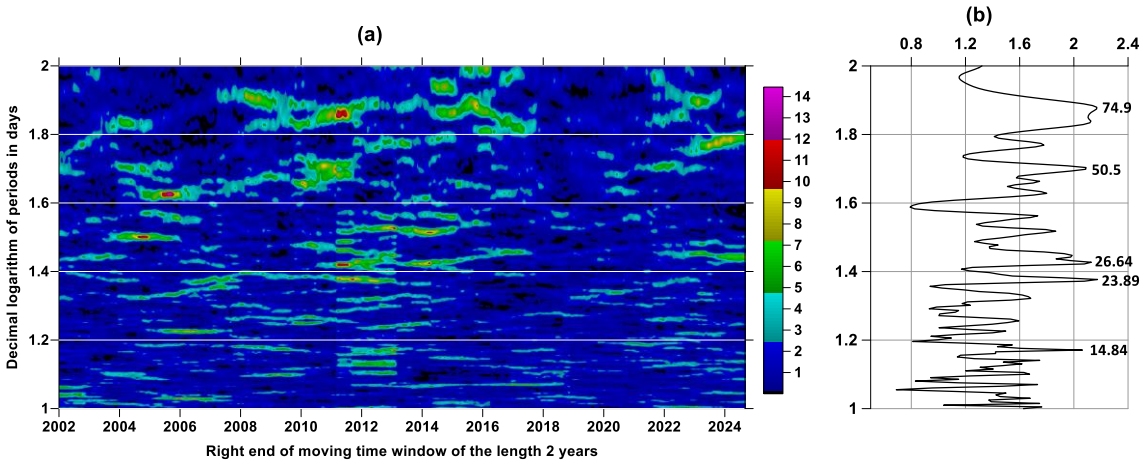

Figure 4. (a) – frequency-time diagram of the evolution of the increment of the logarithmic likelihood function in a sliding time window of 2 years; (b) – graph of the average values of the increment of the logarithmic likelihood function from all time windows, the period in days is shown next to the 5 largest spectral peaks.

 doi:10.20944/preprints202503.2031.v1

Figure 4(b) shows the graph of averaging the increments of the logarithmic likelihood function (5) for all time windows and highlights 5 "spectral" peaks exceeding level 2 with periods of 14.84, 23.89, 26.64, 50.5 and 74.9 days. For them, the peak values of the average increments $\Delta \ln L$ are 2.08, 2.14, 2.15, 2.09 and 2.17, respectively. Using the asymptotic formula (9), we obtain the following probabilities of difference between the periodic components of the seismic regime with these periods and a purely random Poisson process: 0.875, 0.882, 0.883, 0.863 and 0.886.

Thus, it can be stated that the sequence of time moments of earthquakes with magnitudes not lower than 6.5 contains a periodic component with a period of 26.64 days, close to the period of the Sun's rotation with a probability of not less than 0.883. This fact confirms the hypothesis about the influence of solar activity on the Earth's seismicity.

5. Method for Assessing the Measure of Mutual Advance of Two Streams of Events

In the future, we will be interested in the question of whether there is an advance of the moments of time of the largest local maxima of the average values of the proton flux density (Figure 2(a)) relative to the moments of time of earthquakes (Figure 2(b)). Clarification of this question requires also an assessment of the "reverse" advance and calculation of their difference. If the average value of this difference is positive, then there is a trigger effect of the proton flux on seismicity. In addition, the value of the average difference of the advance measures will give a measure of the trigger effect.

To clarify this issue, we applied the influence matrix method proposed in [40] to assess the degree of influence of earthquake sequences on each other in several seismically active regions. In its original implementation, this method is multidimensional. However, below it is simplified and modified for the practically important situation of two time sequences. This modification was previously used in [41–45] to analyze the relationships between seismic event times and local extremum time points of various microseismic background statistics, magnetic field fluctuations, ground tremor, and meteorological time series properties.

Let $t_j^{(\alpha)}$, $j = 1,..., N_\alpha$; $\alpha = 1,2$ represent the moments of time of 2 sequences of events. In our case, these are:

1) a sequence of time moments corresponding to the largest local maxima of the average values of the proton flux;

2) sequence of times of seismic events with magnitude of at least 6.5.

Let us represent their intensities as follows:

$$\lambda^{(\alpha)}(t) = b_0^{(\alpha)} + \sum_{k=1}^{2} b_k^{(\alpha)} \cdot g^{(k)}(t) \tag{10}$$

where $b_0^{(\alpha)} \geq 0, b_\beta^{(\alpha)} \geq 0$ are parameters, $g^{(\beta)}(t)$ - function of influence of time moment $t_j^{(\beta)}$ of the sequence with number β:

$$g^{(\beta)}(t) = \sum_{t_j^{(\beta)} < t} e^{-(t - t_j^{(\beta)})/\tau} \tag{11}$$

According to formula (11), the weight of the event with number j becomes non-zero for times $t > t_j^{(\beta)}$ and decays with characteristic time τ. The parameter $b_\beta^{(\alpha)}$ determines the degree of influence of the flow β on the flow α. The parameter $b_\alpha^{(\alpha)}$ determines the degree of influence of the flow α on itself (self-excitation), and the parameter $b_0^{(\alpha)}$ reflects a purely random (Poisson) component of intensity. Let us fix the parameter τ and consider the problem of determining the parameters $b_0^{(\alpha)}, b_\beta^{(\alpha)}$.

The log-likelihood function for a non-stationary Poisson process is equal to over the time interval $[0, T]$ [38]:

$$\ln(L_\alpha) = \sum_{j=1}^{N_\alpha} \ln(\lambda^{(\alpha)}(t_j^{(\alpha)})) - \int_0^T \lambda^{(\alpha)}(s) ds, \quad \alpha = 1,2 \tag{12}$$

 doi:10.20944/preprints202503.2031.v1

It is necessary to find the maximum of functions (12) with respect to the parameters $b_0^{(\alpha)}, b_\beta^{(\alpha)}$. Taking into account formula (12), we can write the derivative of the logarithmic likelihood function with respect to the parameters:

$$\frac{\partial \ln(L_\alpha)}{\partial b_0^{(\alpha)}} = \sum_{j=1}^{N_\alpha} \frac{1}{\lambda^{(\alpha)}(t_j^{(\alpha)})} - \int_0^T ds, \quad \frac{\partial \ln(L_\alpha)}{\partial b_\beta^{(\alpha)}} = \sum_{j=1}^{N_\alpha} \frac{g^{(\beta)}(t)}{\lambda^{(\alpha)}(t_j^{(\alpha)})} - \int_0^T g^{(\beta)}(s)ds \tag{13}$$

from where and from formula (10) it follows:

$$b_0^{(\alpha)} \frac{\partial \ln(L_\alpha)}{\partial b_0^{(\alpha)}} + \sum_{\beta=1}^{2} b_\beta^{(\alpha)} \frac{\partial \ln(L_\alpha)}{\partial b_\beta^{(\alpha)}} = \sum_{j=1}^{N_\alpha} \left\{ \frac{b_0^{(\alpha)} + \sum_{k=1}^{2} b_k^{(\alpha)} \cdot g^{(k)}(t)}{\lambda^{(\alpha)}(t_j^{(\alpha)})} \right\} - \tag{14}$$

$$-\int_0^T (b_0^{(\alpha)} + \sum_{k=1}^{2} b_k^{(\alpha)} \cdot g^{(k)}(s))ds = N_\alpha - \int_0^T \lambda^{(\alpha)}(s)ds$$

Since the parameters $b_0^{(\alpha)}, b_\beta^{(\alpha)}$ must be non-negative, each term in the leftmost part of this formula is equal to zero at the point of maximum of function (12) – either due to the necessary conditions of the extremum (if the parameters are positive), or, if the maximum is reached at the boundary, then the parameters themselves are equal to zero. Consequently, at the point of maximum of the likelihood function, the equality is satisfied:

$$\int_0^T \lambda^{(\alpha)}(s)ds = N_\alpha \tag{15}$$

Let's substitute the expression $g^{(\beta)}(t)$ from (11) into (15) and divide by T. Then we get another form of formula (15):

$$b_0^{(\alpha)} + \sum_{\beta=1}^{2} b_\beta^{(\alpha)} \cdot \bar{g}^{(\beta)} = \lambda_0^{(\alpha)} \equiv N_\alpha / T \tag{16}$$

where

$$\bar{g}^{(\beta)} = \int_0^T g^{(\beta)}(s)ds / T \tag{17}$$

Substituting $b_0^{(\alpha)}$ from (16) into (12), we obtain the following maximum problem:

$$\Psi^{(\alpha)}(b_1^{(\alpha)}, b_2^{(\alpha)}) = \sum_{j=1}^{N_\alpha} \ln(\lambda_0^{(\alpha)} + \sum_{\beta=1}^{2} b_\beta^{(\alpha)} \cdot \Delta g^{(\beta)}(t_j^{(\alpha)})) \to \max \tag{18}$$

where $\Delta g^{(\beta)}(t) = g^{(\beta)}(t) - \bar{g}^{(\beta)}$, under restrictions:

$$b_1^{(\alpha)} \geq 0, b_2^{(\alpha)} \geq 0, \sum_{\beta=1}^{2} b_\beta^{(\alpha)} \bar{g}^{(\beta)} \leq \lambda_0^{(\alpha)} \tag{19}$$

Function (18) is convex with negative definite Hessian [40] and, therefore, problem (18-19) has a unique solution. Having solved problem (18-19) numerically for a given τ, we can introduce the elements of the influence matrix $\kappa_\beta^{(\alpha)}, \alpha = 1,2; \ \beta = 0,1,2$ according to the formulas:

$$\kappa_0^{(\alpha)} = b_0^{(\alpha)} / \lambda_0^{(\alpha)} \geq 0, \quad \kappa_\beta^{(\alpha)} = b_\beta^{(\alpha)} \cdot \bar{g}^{(\beta)} / \lambda_0^{(\alpha)} \geq 0 \tag{20}$$

The quantity $\kappa_0^{(\alpha)}$ is a share of the average intensity $\lambda_0^{(\alpha)}$ of the process with number α, which is purely stochastic, the part $\kappa_\alpha^{(\alpha)}$ is caused by the influence of self-excitation $\alpha \to \alpha$ and $\kappa_\beta^{(\alpha)}, \beta \neq \alpha$ is determined by the external influence $\beta \to \alpha$. From formula (16) follows the normalization condition:

$$\kappa_0^{(\alpha)} + \sum_{\beta=1}^{2} \kappa_\beta^{(\alpha)} = 1, \quad \alpha = 1,2 \tag{21}$$

As a result, we can determine the influence matrix:

 doi:10.20944/preprints202503.2031.v1

$$\begin{pmatrix} \kappa_0^{(1)} & \kappa_1^{(1)} & \kappa_2^{(1)} \\ \kappa_0^{(2)} & \kappa_1^{(2)} & \kappa_2^{(2)} \end{pmatrix} \quad (22)$$

The first column of matrix (22) is composed of Poisson shares of mean intensities. The diagonal elements of the right submatrix of size 2×2 consist of self-excited elements of mean intensity, while the off-diagonal elements correspond to mutual excitation. The sums of the component rows of the influence matrix (22) are equal to 1. The influence matrices are estimated in a certain sliding time window of length with offset and with a given value of the attenuation parameter τ.

When analyzing variations of the components of influence matrices in sliding time windows corresponding to the mutual influence of the analyzed time sequences, the main attention is paid to their local maxima with their subsequent averaging. Let M_L be the number of windows lengths within limits from $L_{\min}$ up to $L_{\max}$. Thus, the sequence of windows lengths is $L_j = L_{\min} + (j-1)\Delta L,\ j = 1,...,M_L$, where $\Delta L = (L_{\max} - L_{\min})/(M_L - 1)$. Each time window of the length L_j is shifted along time axis with mutual shift Δt. Let $t_k(L_j)$ be the sequence of time moments corresponding to right ends of time windows of the length L_j. The number $K(L_j)$ of time moments $t_k(L_j)$ is defined by mutual shift Δt of time windows of the length L_j. Let $(t_k(L_j), c_k^{(1)}(L_j))$ and $(t_k(L_j), c_k^{(2)}(L_j))$ be elements $\kappa_2^{(1)}$ and $\kappa_1^{(2)}$ of the matrix (22), corresponding to mutual influences $2 \to 1$ and $1 \to 2$ of analyzed time moments for current position $t_k(L_j)$ of time window of the length L_j. Let $(t_k^*(L_j), \hat{c}_k^{(\alpha)}(L_j))$, $\alpha = 1,2$ be local maxima of $c_k^{(\alpha)}(L_j)$, i.e. $c_{k-1}^{(\alpha)}(L_j)) < \hat{c}_k^{(\alpha)}(L_j) < c_{k+1}^{(\alpha)}(L_j)$.

Let's take some "small" time interval of the length η and for the sequence of time moments $[\nu_m, \nu_{m+1}]$, $\nu_{m+1} - \nu_m = \eta$ of such time fragments we will calculate the mean values $G_{2\to1}(\nu_{m+1})$ and $G_{1\to2}(\nu_{m+1})$ of $\hat{c}_k^{(\alpha)}(L_j)$ for which their time marks $t_k^*(L_j)$ belong to these fragments. Averaging is performed over all time window lengths $L_j,\ j = 1,...,M_L$. These mean values in dependence on right end of intervals ν_{m+1} gives the measures of averaged effects of advance of 2nd sequence of time moments with respect to the 1st one and vice versa. Our main purpose is calculating the difference $\Delta G(\nu_{m+1}) = G_{2\to1}(\nu_{m+1}) - G_{1\to2}(\nu_{m+1})$. In this formula the 1st sequence is the sequence of time moments of earthquakes with magnitude not less than 6.5 whereas the 2nd sequence are time moments of largest local maxima of mean proton flux time series. Thus, if average $< \Delta G(\nu_{m+1}) >$ is positive it means that there is a trigger effect.

The full set of parameters of the method is the following: τ, $L_{\min}$, $L_{\max}$, M_L, Δt, η. In our calculations we used $\tau = 0.05$ year (approximately 18 days), $L_{\min} = 0.5$ year, $L_{\max} = 1$ year, $M_L = 100$, $\Delta t = 1$ day, $\eta = 0.1$ year. The calculation results are most sensitive to the choice of parameters τ, $L_{\min}$, $L_{\max}$. The values used were chosen as a result of trial calculations and selection of the best options.

6. Measures of Mutual Advance of Local Maxima of the Average Value of Proton Flux Density and Seismic Event Sequence

In this section of the paper we apply the method described earlier to the analysis of the relationships between the time sequences presented in Figure 2. Figure 5 presents the results of such an analysis.

 doi:10.20944/preprints202503.2031.v1

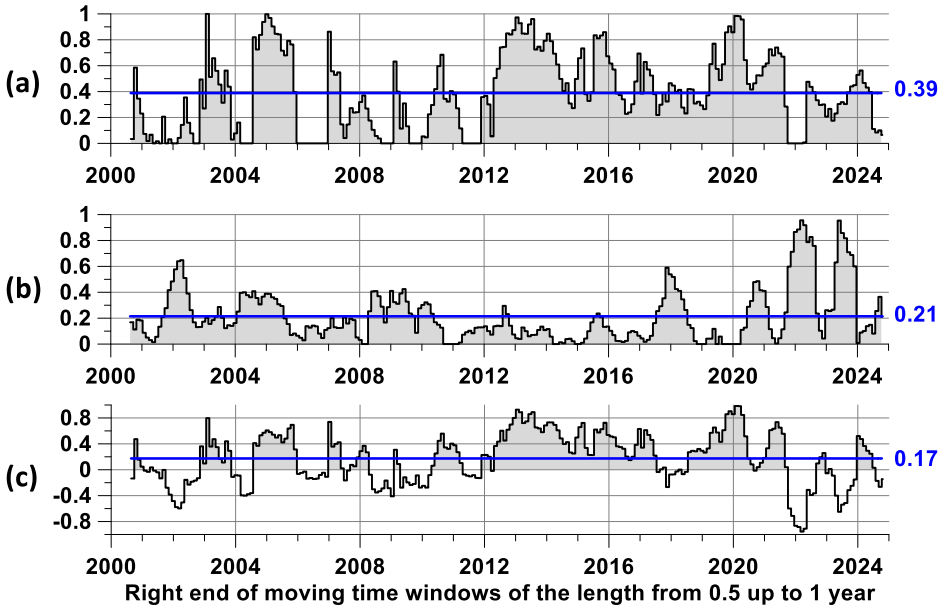

Figure 5. (a) – average values of local maxima of the component of influence matrices corresponding to the "direct" influence of the moments of time of the largest local maxima of the averaged values of the proton flux density on the moments of time of earthquakes with a magnitude of at least 6.5; (b) – average values of local maxima of the component of influence matrices corresponding to the "reverse" influence of the moments of time of earthquakes on the moments of time of the largest local maxima of the averaged values of the proton flux density; (c) – the difference between the average values of local maxima of the component of influence matrices corresponding to the "direct" influence and corresponding to the "reverse" influence. Blue line – average value, their numerical values are indicated on the right.

From the comparison of the graphs in Figure 5 it is evident that the advance of the moments of time of the largest local maxima of the smoothed proton flux relative to the moments of time of earthquakes with a magnitude of not less than 6.5 is on average significantly greater than the reverse advance. At the same time, the difference between the average values of the advance measures, presented in Figure 5(c) has a positive average value equal to 0.17. This value can be interpreted as an estimate of the part of the average intensity of all earthquakes with a magnitude of not less than 6.5 for those seismic events for which the maximum values of the average proton flux density are a trigger. Another numerical characteristic of the trigger effect is the part of the lengths of the time interval for which the difference between the "direct" and "reverse" advance is positive. For the graph in Figure 5(c) this part is equal to 0.62.

7. Proton Flux Density Time Series Statistics

The average proton flux density values used above are the simplest statistics. An idea arises to try other proton time series statistics and to estimate the relationship of the times of their "most expressive" (i.e. largest local maxima or smallest local minima) extreme values with the times of earthquakes using the above model of influence matrices. In addition to the simple average values, we used 5 different proton flux time series statistics described below. These statistics were estimated in the same time windows of 1440 5-minute samples (5 days), taken with an offset of 288 samples (1 day), as before, when calculating the average values.

1) *The kurtosis* of a time series $x(t)$ is calculated in each time window using the formula [46]:

$$\kappa = < (x(t) - m_x)^4 > / \left(< (x(t) - m_x)^2 > \right)^2, \; m_x = < x(t) > \qquad (23)$$

Here, the angle brackets denote the operation of calculating the mean value. The value κ can be considered as a measure of the difference from the Gaussian distribution, for which $\kappa = 3$. Below we will use the logarithm of the kurtosis coefficient: $\lg(\kappa)$.

 doi:10.20944/preprints202503.2031.v1

2) *The minimum wavelet-based normalized entropy* En of a time series $x(t)$ is calculated based on the decomposition of the time series within a window into orthogonal wavelets.

$$En = -\sum_k p_k \cdot \log(p_k)/\log(N). \quad (24)$$

In formula (24) $p_k = c_k^2 / \sum_j c_j^2$, c_k are the wavelet coefficients of the signal $x(t)$, N is the total number of wavelet coefficients. Seventeen orthogonal Daubechies wavelets were used: 10 ordinary bases with a minimum support with a number of vanishing moments from 1 to 10 and 7 so-called Daubechies symlets [47], with a number of vanishing moments from 4 to 10. For each of the bases, the entropy (24) of the distribution of the squares of the wavelet coefficients was calculated, and then, by enumeration, the optimal basis was found that realized the minimum value in each time window. By construction, $0 \le En \le 1$. The details of calculating the entropy (24) in a sliding time window are described in [48].

3) *Wavelet-based spectral slope* β. After determining the optimal orthogonal wavelet from the minimum entropy condition, it is possible to calculate the average values S_k of the squares of the wavelet coefficients at each detail level, which is part of the oscillation energy corresponding to the detail level with the number k, which corresponds to the frequency band with the boundary frequencies $f_{\min}^{(k)} = 1/(2^{(k+1)}\Delta s)$ and $f_{\max}^{(k)} = 1/(2^k \Delta s)$, where Δs is the length of the sampling time interval (in our case Δs = 5 min) [47]. Let us consider the values of the periods corresponding to the centers of these frequency bands:

$$T_k = 2/(f_{\min}^{(k)} + f_{\max}^{(k)}) = 2\Delta s/(2^{-k} + 2^{-(k+1)}). \quad (25)$$

The quantities $S_k = S(T_k)$ are similar to the Fourier power spectra. These quantities are convenient to use when calculating the slope of the graph of the logarithm of the power spectrum as a function of the logarithm of the period. The spectral slope in each time window is found by the least squares method:

$$\sum_k (\ln(S(T_k)) - \beta \cdot \ln(T_k)) - c)^2 \to \min_{\beta, c}, \quad (26)$$

4) The Donoho-Johnston wavelet-based index (DJ-index) γ is defined as the ratio of the number of "large" wavelet coefficients by absolute value to their total number. By definition $0 \le \gamma \le 1$. The threshold separating the "large" wavelet coefficients is $T_{DJ} = \sigma\sqrt{2 \cdot \ln N}$. This threshold separates the informative wavelet coefficients from other coefficients that are considered noisy [47,49]. The value σ is an estimate of the standard deviation of noise under the assumption that the noise is most concentrated at the 1st detail level of the orthogonal wavelet decomposition. To estimate the value, the median estimate of the standard deviation of a normal random variable is used:

$$\sigma = med\left\{\left|c_k^{(1)}\right|, k = 1, ..., N/2\right\}/0.6745, \quad (27)$$

5) The multifractal singularity spectrum support width $\Delta\alpha$ is an important characteristic of the signal and is considered as a measure of the diversity (complexity) of its stochastic behavior. It is defined as $\Delta\alpha = \alpha_{\max} - \alpha_{\min}$, where $\alpha_{\min}$ and $\alpha_{\max}$ are estimates of minimum and maximum values of Holder-Lipschitz exponent [50] α which governs the behavior of the signal at the vicinity of time moment t: $|x(t+\delta/2) - x(t-\delta/2)| \sim |\delta|^{\alpha}$, $\delta \to 0$. For a mono-fractal signal, the Holder-Lipschitz exponent is the same for all time moments t. Otherwise, the signal is multi-fractal and the concept of the spectrum of singularities $F(\alpha)$ is introduced, equal to the fractal dimension of the time moments with the same value of the Holder-Lipschitz exponent, equal to α [51]. To estimate $\Delta\alpha$ in each time window, we used the method of fluctuation analysis after removing scale-dependent trends [52]. The implementation of the method used is described in detail in [48]. To remove local polynomial trends for the proton flux density time series, we used zero-order polynomials, i.e., we analyzed fluctuations after removing local means.

 doi:10.20944/preprints202503.2031.v1

For a sequence of time intervals of 5 days, taken with a shift of 1 day, we calculated the values of all 5 statistics of the proton flux density time series. The results of these calculations are presented in the graphs in Figure 6.

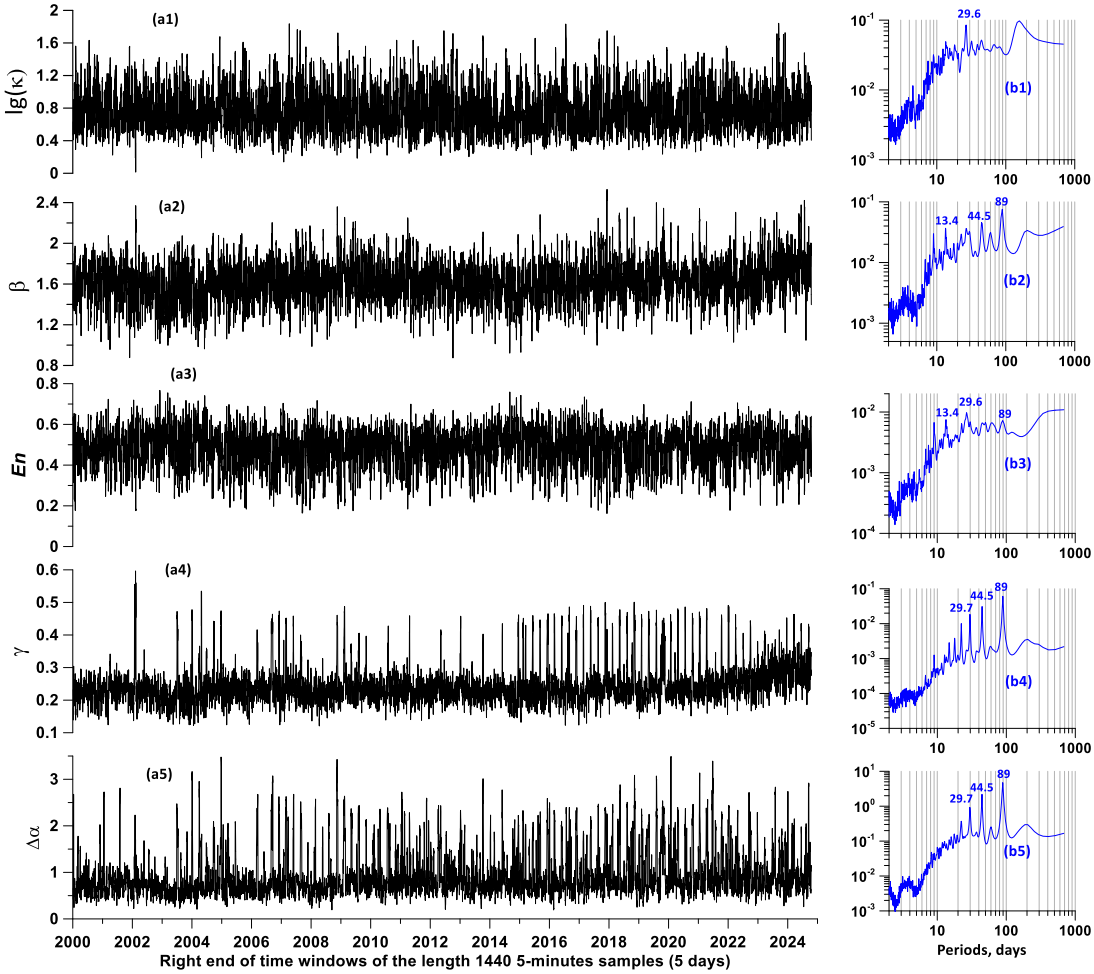

Figure 6. (a1)-(a5) – graphs of time series of 5 proton flux density statistics: logarithm of kurtosis $\lg(\kappa)$, wavelet-based spectral slope β, minimum normalized entropy of wavelet coefficients En, Donoho-Johnstone index γ and the singularity spectrum support width $\Delta\alpha$, calculated in sliding time windows of 5 days with a shift of 1 day. On the right are graphs (b1)-(b5), corresponding to the power spectra of time series of proton flux density statistics, for the largest spectral peaks their periods in days are indicated.

From the graphs of the power spectra of the time series of changes in statistics, it is evident that for all of them, with the exception of $\lg(\kappa)$, there is a periodicity of 89 days, which is especially pronounced for γ and $\Delta\alpha$. It should be noted that the power spectrum of the change in the average values of the proton flux density does not contain a spectral component with a period of 89 days.

Let us consider in more detail the frequency-time structure of the variations in the singularity spectrum support width $\Delta\alpha$ (Figure 6(a5)), for which the 89-day periodicity is most clearly visible. Let us denote $\Delta\alpha(s)$ the dependence of the singularity spectrum carrier width on time (the position of the right end of the 5-day time window with a 1-day offset) s and calculate the Morlet wavelet transform [47]:

$$c_{\Delta\alpha}(t,\upsilon)=\frac{1}{\sqrt{\upsilon}}\int_{-\infty}^{+\infty}\Delta\alpha(s)\cdot\varphi\left(\frac{s-t}{\upsilon}\right)ds,\quad \upsilon>0,\quad \varphi(t)=\frac{1}{\pi^{1/4}}\exp(-t^2/2-i\pi t) \qquad (28)$$

The values $|c_{\Delta\alpha}(t,\upsilon)|^2$ can be interpreted as the energy of signal $\Delta\alpha(s)$ oscillations in the vicinity of a time point t with a period υ. Figure 7(a) shows the Morlet time-frequency diagram of

 doi:10.20944/preprints202503.2031.v1

values $\lg|c_{\Delta\alpha}(t,\upsilon)|$ for 200 values of periods υ varying within the range from 10 to 500 days with a uniform step on a logarithmic scale. For the frequency band with periods from 63 to 158 days (logarithms of periods from 1.8 to 2.2), in which the most intense periodic variations of $\Delta\alpha(s)$ with a central period of 89 days are concentrated, we calculate the maximum values $\max_{\upsilon}\left(\lg|c_{\Delta\alpha}(t,\upsilon)|\right)$.

These maximum values are shown in Figure 7(b) by a black line. The red line in Figure 7(b) shows the cyclic trend for the maximum values of the logarithms of the Morlet wavelet coefficients in the frequency band highlighted above. The period of this oscillation was determined numerically from the condition of minimum variance of deviations for trial cyclic trends with periods in the range from 1500 to 5500 days. As a result of such calculations, it turned out that the optimal period is equal to 4429 days or approximately 12.13 years, that is, very close to the period of solar cycles.

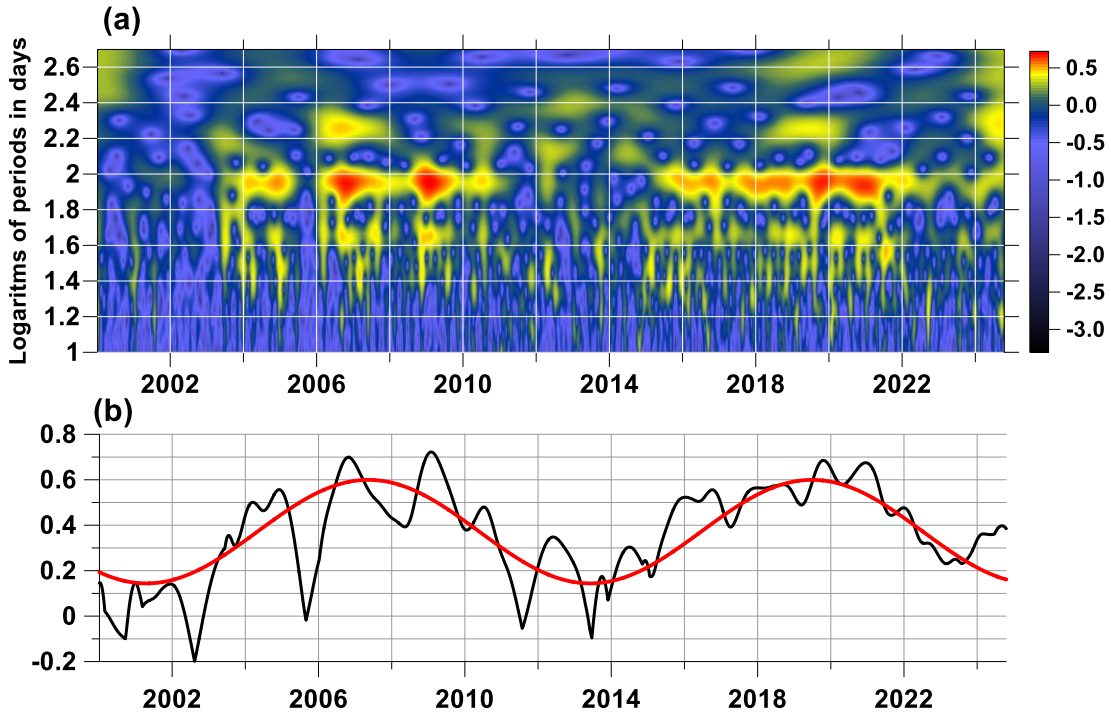

Figure 7. (a) – frequency-time diagram of the logarithms of the moduli of the Morlet wavelet coefficients of the variations of the singularity spectrum support width $\Delta\alpha$ for periods from 10 to 500 days; (b) – the black line represents the maximum values of the logarithms of the moduli of the Morlet coefficients for periods from 63 to 158 days, the red line is the optimal cyclic trend with a period of 4429 days or 12.13 years.

8. Measures of Mutual Advance of Local Extrema of Proton Flux Density and Seismic Event Sequence Statistics

The further plan of using 5 statistics of the proton flux density time series consists in assessing the measures of advancement of the time moments of their most expressive local extrema (the largest local maxima and the smallest local minima) relative to the time moments of earthquakes with a magnitude of at least 6.5. In this case, the number of points of the most expressive local extrema will be chosen equal to the number of seismic events, i.e. 1136.

To eliminate the influence of low-frequency components of the change in the values of statistics on the determination of the moments of time of local extremes, the time series, the graphs of which are presented in Figure 6 (a1-a5), were subjected to the operation of removing low frequencies using Gaussian kernel smoothing. Let $u(t)$ be a time series with discrete time t. Gaussian kernel averaging of a time series $u(t)$ with radius (scale parameter) $h>0$ at the moment of time t, is calculated using the formula [53]:

 doi:10.20944/preprints202503.2031.v1

$$\bar{u}(t \mid h) = \sum_s u(s) \cdot e^{-\left(\frac{t-s}{h}\right)^2} \Big/ \sum_s e^{-\left(\frac{t-s}{h}\right)^2} \qquad (29)$$

Calculation of the kernel averaging by formula (32) for long time series can be effectively implemented using the fast Fourier transform. Then the average values of the time series for the averaging radius h equal to 2 days were subtracted from the time series of changes in statistics and the most expressive points of local extrema were found for the residuals. These operations are illustrated by the graphs in Figure8.

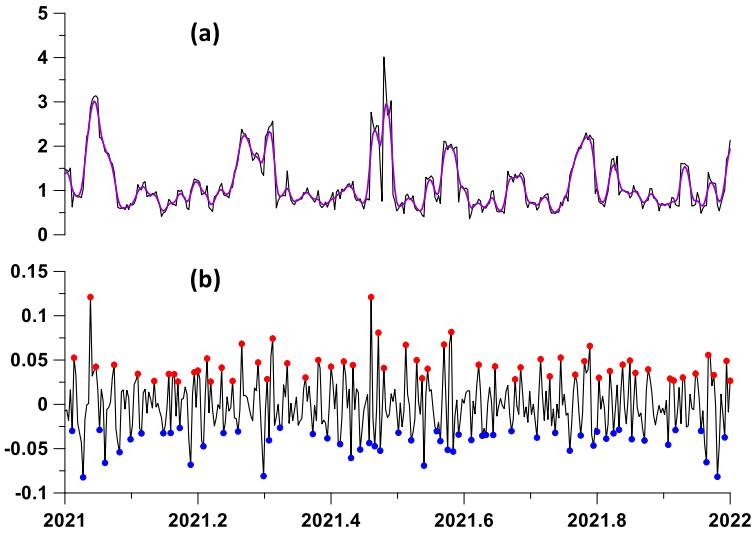

Figure 8. (a) – the black line shows a graph of a fragment of the time series of changes in singularity spectrum support width $\Delta\alpha$ for the time interval 2021-2022; the purple line is the smoothing of the time series by a Gaussian kernel of radius 2 days. In Figure (b), the red and blue dots show the positions of 1136 largest local maxima and minima of the difference between the original changes in statistics $\Delta\alpha$ and the smoothed values (black line) in this time fragment.

When estimating the advance measures by the points of local extrema of the proton flux statistics, we tested both the points of the largest local maxima and the points of the smallest local minima after excluding low frequencies using Gaussian smoothing (29). In this case, the differences between the "direct" and "reverse" lead were calculated. Then, the variant of the largest local maxima and the smallest local minima for which the average value of the difference between the average measures of the "direct" and "reverse" lead was maximum was selected. As a result of such an enumeration of variants, it turned out that the most preferable are the smallest points of local minima for the statistics $\lg(\kappa)$, β, γ and $\Delta\alpha$, whereas the largest local maxima for the entropy En. The results of estimating the differences in the lead measures are presented in Figure 9.

It is interesting to note that when analyzing the prognostic properties of low-frequency seismic noise measured by a global network of 229 broadband seismic stations located around the world, it turned out that it is the points of the smallest local minima of statistics γ, $\Delta\alpha$ and the points of the largest local maxima of entropy En that have the maximum prognostic effects relative to the times of the strongest earthquakes with magnitudes of at least 7 [41].

Preprints.org (www.preprints.org) | NOT PEER-REVIEWED | Posted: 27 March 2025 doi:10.20944/preprints202503.2031.v1

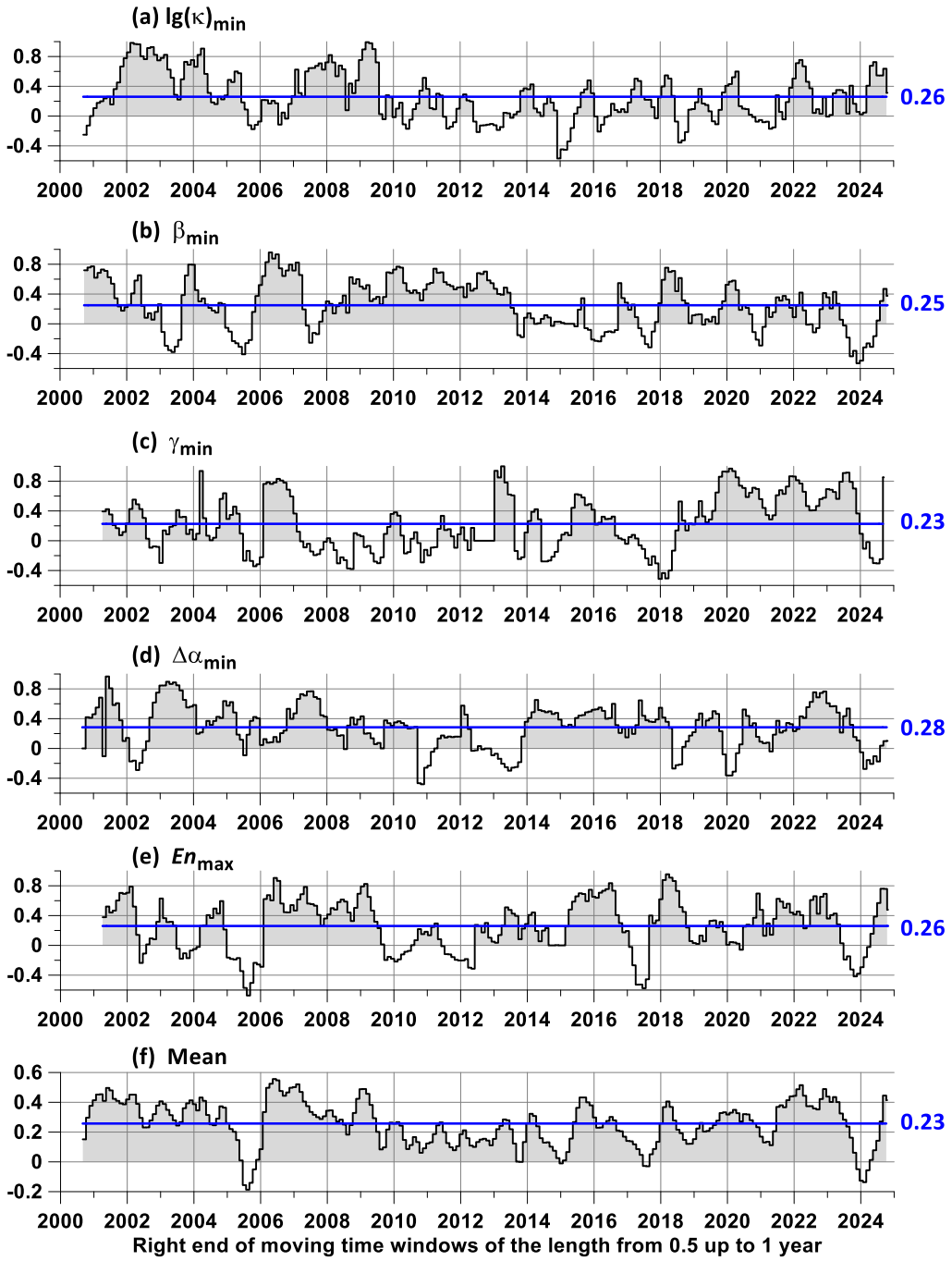

Figure 9. Figure (a)-(e) presents graphs of differences between average values of local extrema of components of influence matrices corresponding to "direct" advance of time points of local extrema of 5 proton flux density statistics relative to time moments of earthquakes with magnitude not lower than 6.5 and corresponding to "reverse" determination. Graphs (a-d) are constructed respectively for local minima of logarithm of kurtosis $\lg(\kappa)$, spectral slope β, Donoho-Johnstone index γ and singularity spectrum support width $\Delta\alpha$; graph (e) – for points of local maxima of entropy En. Graph (f) is averaging of curves in graphs (a-e). Blue lines are average values, their numerical values are indicated on the right.

From the point of view of the average value of the difference in the advance measures, all these results are noticeably better than using the simplest statistics – the average value of the proton flux density (Figure 5(c)). In this case, the best result is achieved when using the minimum $\Delta\alpha$ values – the multi-fractal singularity spectrum support width, for which the average value is 0.28.

Another characteristic of the difference of average lead measures is the part of interval lengths with positive values of the difference. This characteristic is equal to: $\lg(\kappa)_{\min}$ – 0.78; $\beta_{\min}$ – 0.75; $\gamma_{\min}$

 doi:10.20944/preprints202503.2031.v1

– 0.71; $\Delta\alpha_{min}$ – 0.83; En_{max} – 0.76; *Mean* – 0.95, that is, the use of averaging provides a frequent positive value of the lead measure, although it loses out in comparison with the average value of using minima $\Delta\alpha$.

9. Discussion

As a result of the analysis, the trigger effect of the proton flux on the Earth's seismicity was proven. A quantitative estimate of the share of the average intensity of earthquakes with a magnitude of at least 6.5, for which the proton flux is a trigger, was obtained - it is equal to 0.28.

An 89-day periodicity in the variations of proton flux statistics has been revealed. One hypothesis is that this periodicity may be related to the modulation of the proton flux density by the motion of Mercury, the planet closest to the Sun with an orbital period of 89 days. The presence of a 12-year periodicity in the change in the maximum values of the logarithms of the modules of the Morlet wavelet coefficients for the singularity spectrum support width confirms the connection of the 89-day periodicity with solar dynamics. Another hypothesis for the origin of this periodicity is the coincidence of 89 days with half the oscillation period of the SOHO satellite, which measures the proton flux density, in the vicinity of the Lagrange libration point L1 [32]. However, the mechanism of such modulation, which is maximum precisely for the Donoho-Johnston index statistics and the singularity spectrum support width, remains unclear.

Author Contributions: A.L.—ideating the research, writing the text, data processing; E.R.— data preparation. All authors have read and agreed to the published version of the manuscript.

Funding: This research received no external funding.

Institutional Review Board Statement: Not applicable.

Informed Consent Statement: Not applicable.

Data Availability Statement: The proton flux data were available from the site https://soho.nascom.nasa.gov/data/data.html . The data of earthquakes sequence are available from the site https://earthquake.usgs.gov/earthquakes/search/.

Acknowledgments: This work was carried out within the framework of the state assignments of the Institute of Physics of the Earth of the Russian Academy of Sciences.

Conflicts of Interest: The authors declare that the research was conducted in the absence of any commercial or financial relationships that could be construed as a potential conflict of interest.

References

1. Singh A.K., Bhargawa A., Siingh D., Singh R.P. Physics of Space Weather Phenomena: A Review. *Geoscience*, **2021**, 11, 286. https://doi.org/10.3390/geosciences11070286
2. Kokorowski, M., A. Seppälä, J. G. Sample, R. H. Holzworth, M. P. McCarthy, E. A. Bering, and E. Turunen, Atmosphere-ionosphere conductivity enhancements during a hard solar energetic particle event, *J. Geophys. Res*. **2012**, 117, A05319, https://doi.org/10.1029/2011JA017363
3. Kutiev I., Tsagouri I., Perrone L., Pancheva D., Mukhtarov P., Mikhailov A.,Lastovicka J., Jakowski N., Buresova D., Blanch E., Andonov B., Altadil D.l, Magdaleno S., Paris M., and Torta J.M. Solar activity impact on the Earth's upper atmosphere. *J. Space Weather Space Clim.* **2013**, 3, A06, https://doi.org/10.1051/swsc/2013028
4. Elias, A.G.; de Haro Barbas, B.F.; Zossi, B.S.; Medina, F.D.; Fagre, M.; Venchiarutti, J.V. Review of Long-Term Trends in the Equatorial Ionosphere Due the Geomagnetic Field Secular Variations and Its Relevance to Space Weather. *Atmosphere* **2022**, 13, 40. https://doi.org/10.3390/atmos13010040
5. Laurenza, M., E. W. Cliver, J. Hewitt, M. Storini, A. G. Ling, C. C. Balch, and M. L. Kaiser, A technique for short-term warning of solar energetic particle events based on flare location, flare size, and evidence of particle escape, *Space Weather* **2009**, 7, S04008, https://doi.org/doi:10.1029/2007SW000379

 doi:10.20944/preprints202503.2031.v1

6. Anastasiadis A., Papaioannou A., Sandberg I., Georgoulis M., Tziotziou K., Kouloumvakos A. & Jiggens P. Predicting Flares and Solar Energetic Particle Events: The FORSPEF Tool. *Sol Phys* **2017**, 292, 134. https://doi.org/10.1007/s11207-017-1163-7
7. Aminalragia-Giamini S., Jiggens P., Anastasiadis A., Sandberg I., Aran A., Vainio R., Papadimitriou C., Papaioannou A., Tsigkanos A., Paouris E., Vasalos G., Paassilta M. and Dierckxsens M. Prediction of Solar Proton Event Fluence spectra from their Peak flux spectra. *J. Space Weather Space Clim.* **2020**, 10, 1–16. https://doi.org/10.1051/swsc/2019043
8. Alberti, T., Consolini, G., & Marcucci, M. F. Open issues in statistical forecasting of solar proton events: A machine learning perspective. *Space Weather* **2021**, 19, e2021SW002794. https://doi.org/10.1029/2021SW002794
9. Pulinets, S.A., Boyarchuk, K. *Ionospheric Precursors of Earthquakes*; **2004**, Springer: Berlin/Heidelberg, Germany.
10. Huzaimy, J.; Yumoto, K. Possible correlation between solar activity and global seismicity. *In Proceeding of the 2011 IEEE International Conference on Space Science and Communication (IconSpace)*, Penang, Malaysia, 12–13 July **2011**; pp. 138–141 https://doi.org/10.1109/IConSpace.2011.6015869
11. Tavares M., Azevedo A. Influences of solar cycles on earthquakes. *Nat. Sci.* **2011**, 3, 436. http://dx.doi.org/10.4236/ns.2011.36060
12. Anagnostopoulos G., Spyroglou I., Rigas A.,Preka-Papadema P., Mavromichalaki H., and Kiosses I. The sun as a significant agent provoking earthquakes. *Eur. Phys. J. Special Topics* **2021**, 230, 287-333. https://doi.org/10.1140/epjst/e2020-000266-2
13. Sobolev G.A. The Effect of Strong Magnetic Storms on the Occurrence of Large Earthquakes. *Izv., Phys. Solid Earth*, 2021, 57, 20–36. https://doi.org/10.1134/S1069351321010080
14. Ouzounov D., Khachikyan G. Studying the Impact of the Geospace Environment on Solar Lithosphere Coupling and Earthquake Activity. *Remote Sens.* **2024**, 16, 24. https://doi.org/10.3390/rs16010024
15. Saldanha, M.H.J., Hirata, Y. Solar activity facilitates daily forecasts of large earthquakes. *Chaos Interdiscip. J. Nonlinear Sci.* **2022**, 32, 061107. https://doi.org/10.1063/5.0096150
16. Pulinets, S., Khachikyan, G. The Global Electric Circuit and Global Seismicity. *Geosciences* **2021**, 11, 491. https://doi.org/10.3390/geosciences11120491
17. Marchetti D., De Santis A., Campuzano S.A., Zhu K., Soldani M., D'Arcangelo S., Orlando M., Wang T., Cianchini G., Di Mauro D., Ippolito A., Nardi A., Sabbagh D., Chen W., He X., Shen X., Wen J., Zhang D., Zhang H., Yiqun Zh. and Zeren Zh. Worldwide Statistical Correlation of Eight Years of Swarm Satellite Data with M5.5+ Earthquakes: New Hints about the Preseismic Phenomena from Space. *Remote Sens.* **2022**, 14, 2649. https://doi.org/10.3390/rs14112649
18. Marchitelli V, Harabaglia P, Troise C & De Natale G. On the correlation between solar activity and large earthquakes worldwide. *Scientific Reports* **2020**, 10:11495, https://doi.org/10.1038/s41598-020-67860-3
19. Marchitelli V, Troise C, Harabaglia P, Valenzano B and De Natale G. On the Long Range Clustering of Global Seismicity and its Correlation With Solar Activity: A New Perspective for Earthquake Forecasting. *Front. Earth Sci.* **2020**, 8:595209. https://doi.org/10.3389/feart.2020.595209
20. Novikov V., Ruzhin, Y., Sorokin V., Yaschenko A. Space weather and earthquakes: Possible triggering of seismic activity by strong solar flares. *Ann. Geophys.* **2020**, 63, PA554. http://dx.doi.org/10.4401/ag-7975
21. Novikov, V.A., Sorokin, V.M. Electromagnetic Trigger Effects in the Ionosphere-Atmosphere-Lithosphere System and Their Possible Use for Short-Term Earthquake Forecasting. *Izv., Phys. Solid Earth* **2024**, 60, 879-890. https://doi.org/10.1134/S1069351324700800
22. Sorokin V., Yaschenko A., Mushkarev G., Novikov V. Telluric Currents Generated by Solar Flare Radiation: Physical Model and Numerical Estimations. *Atmosphere* **2023**, 14, 458. https://doi.org/10.3390/atmos14030458
23. Sorokin V., Novikov V. Possible Interrelations of Space Weather and Seismic Activity: An Implication for Earthquake Forecast. *Geosciences* **2024**, 14, 116. https://doi.org/10.3390/geosciences14050116
24. Zeigarnik V.A., Bogomolov L.M. & Novikov V.A. Electromagnetic Earthquake Triggering: Field Observations, Laboratory Experiments, and Physical Mechanisms - A Review. *Izv., Phys. Solid Earth* **2022**, 58, 30-58. https://doi.org/10.1134/S1069351322010104

 doi:10.20944/preprints202503.2031.v1

25. Altaibek, A.; Nurtas, M.; Zhantayev, Z.; Zhumabayev, B.; Kumarkhanova, A. Classifying Seismic Events Linked to Solar Activity: A Retrospective LSTM Approach Using Proton Density. *Atmosphere* **2024**, 15, 1290. https://doi.org/10.3390/atmos15111290
26. Wing S. and Johnson J.R. Applications of Information Theory in Solar and Space Physics. *Entropy* **2019**, 21, 140; https://doi.org/10.3390/e21020140
27. Wing, S.; Johnson, J.; Vourlidas, A. Information theoretic approach to discovering causalities in the solar cycle. *The Astrophysical Journal* **2018**, 854:85. https://doi.org/10.3847/1538-4357/aaa8e7
28. Consolini G., Tozzi R., and De Michelis P. Complexity in the sunspot cycle. *Astronomy & Astrophysics*, **2009**, 506, 1381-1391, https://doi.org/10.1051/0004-6361/200811074
29. Balasis, G.; Boutsi, A.Z.; Papadimitriou, C.; Potirakis, S.M.; Pitsis, V.; Daglis, I.A.; Anastasiadis, A.; Giannakis, O. Investigation of Dynamical Complexity in Swarm-Derived Geomagnetic Activity Indices Using Information Theory. *Atmosphere* **2023**, 14, 890. https://doi.org/10.3390/atmos14050890
30. Papadimitriou C., Balasis G., Boutsi A.Z., Daglis I.A., Giannakis O., Anastasiadis A., De Michelis P. and Consolini G. Dynamical Complexity of the 2015 St. Patrick's Day Magnetic Storm at Swarm Altitudes Using Entropy Measures. *Entropy* **2020**, 22, 574; https://doi.org/10.3390/e22050574
31. Boutsi, A.Z.; Papadimitriou, C.; Balasis, G.; Brinou, C.; Zampa, E.; Giannakis, O. Dynamical Complexity in Geomagnetically Induced Current Activity Indices Using Block Entropy. *Entropy* **2025**, 27, 172. https://doi.org/10.3390/e27020172
32. Craig R. E. Long Term Missions at the Sun-Earth Libration Point L1: ACE, SOHO, and WIND. *AAS 11-485GSFC.CP.4786.2011AAS/AIAA Astrodynamics Specialist Conference*; Jul 31, **2011** - Aug 04, **2011**; Girdwood, AK; United States https://api.core.ac.uk/oai/oai:casi.ntrs.nasa.gov:20110022484
33. SOHO data. Available online https://soho.nascom.nasa.gov/data/data.html (accessed on 02 February 2025)
34. USGS Search Earthquake Catalog. Available online: https://earthquake.usgs.gov/earthquakes/search/ (accessed on 02 February 2025).
35. Marple S.L. (Jr) *Digital spectral analysis with applications*. **1987**, Prentice-Hall, Inc., Englewood Cliffs, New Jersey.
36. Lyubushin A.A., V.F.Pisarenko, V.V.Ruzich and V.Yu.Buddo, A New Method for Identifying Seismicity Periodicities. *Volcanology and Seismology*, **1998**; 20:73-89.
37. Lyubushin, A. *Entropy of GPS-measured Earth tremor*, **2024**, Chapter from the edited volume "Revolutionizing Earth Observation - New Technologies and Insights". http://dx.doi.org/10.5772/intechopen.1004399
38. Cox, D.R.; Lewis, P.A.W., **1966**, The Statistical Analysis of Series of Events; Methuen: London, UK,
39. Rao C.R. *Linear statistical inference and its applications*, **1965**, John Wiley & Sons, Inc. N.Y., London, Sydney.
40. Lyubushin A.A., Pisarenko V.F. Research on Seismic Regime Linear Model of Intensity of Interacting Point Processes. *Physics of the Solid Earth, English Translation*, **1994**, 29, 12, 1108-1113.
41. Lyubushin, A. Investigation of the Global Seismic Noise Properties in Connection to Strong Earthquakes. *Front. Earth Sci.* **2022**, *10*, 905663. https://doi.org/10.3389/feart.2022.905663 .
42. Lyubushin, A.; Rodionov, E. Wavelet-based correlations of the global magnetic field in connection to strongest earthquakes. *Adv. Space Res.* **2024**, *74*, 3496–3510. https://doi.org/10.1016/j.asr.2024.06.046 .
43. Lyubushin, A.; Rodionov, E. Prognostic Properties of Instantaneous Amplitudes Maxima of Earth Surface Tremor. *Entropy* **2024**, *26*, 710. https://doi.org/10.3390/e26080710 .
44. Lyubushin, A.; Kopylova, G.; Rodionov, E.; Serafimova, Y. An Analysis of Meteorological Anomalies in Kamchatka in Connection with the Seismic Process, *Atmosphere* **2025**, 16, 78. https://doi.org/10.3390/atmos16010078
45. Lyubushin, A.; Kopylova, G.; Rodionov, E.; Serafimova, Y. An Analysis of Meteorological Anomalies in Kamchatka in Connection with the Seismic Process, *Atmosphere* **2025**, 16, 78. https://doi.org/10.3390/atmos16010078
46. Kendall, M.G. and Stuart, A. *The Advanced Theory of Statistics*, *Vol. 1*, **1977**, London: Charles Griffin and Co.
47. Mallat, S.A. *Wavelet Tour of Signal Processing*, 2nd ed., **1999**, Academic Press: Cambridge, MA, USA.
48. Lyubushin A. Low-Frequency Seismic Noise Properties in the Japanese Islands, *Entropy* **2021**, 23, 474. https://doi.org/10.3390/e23040474

 doi:10.20944/preprints202503.2031.v1

49. Donoho, D.L. and Johnstone, I.M., Adapting to unknown smoothness via wavelet shrinkage, *J. Am. Stat. Assoc.*, **1995**, 90(432), 1200-1224.
50. Taqqu M.S., Self-similar processes. In *Encyclopedia of Statistical Sciences*, **1988**, vol.8, Wiley, New York, NY, 352-357.
51. Feder J., *Fractals*, **1988**, Plenum Press, New York, London.
52. Kantelhardt, J.W., Zschiegner, S.A., Konscienly-Bunde, E., Havlin, S., Bunde, A., and Stanley, H.E., Multifractal detrended fluctuation analysis of nonstationary time series, *Phys. A*, **2002**, 316(1-4), 87-114.
53. Hardle W., *Applied Nonparametric Regression*. (Biometric Society Monographs No. 19.), **1990**, Cambridge University Press, Cambridge.